# Multivariate Self-Organizing Map Approach to Classifying Supercell Tornado Environments Using Near-Storm, Low-Level Wind and Thermodynamic Profiles

CHRISTOPHER J. NOWOTARSKI

*Department of Atmospheric Sciences, Texas A&M University, College Station, Texas*

ERIN A. JONES

*Department of Earth Sciences, Millersville University, Millersville, Pennsylvania*

(Manuscript received 22 December 2017, in final form 6 February 2018)

ABSTRACT

Self-organizing maps (SOMs) have been shown to be a useful tool in classifying meteorological data. This paper builds on earlier work employing SOMs to classify model analysis proximity soundings from the near-storm environments of tornadic and nontornadic supercell thunderstorms. A series of multivariate SOMs is produced wherein the input variables, height, dimensions, and number of SOM nodes are varied. SOMs including information regarding the near-storm wind profile are more effective in discriminating between tornadic and nontornadic storms than those limited to thermodynamic information. For the best-performing SOMs, probabilistic forecasts derived from matching near-storm environments to a SOM node may provide modest improvements in forecast skill relative to existing methods for probabilistic forecasts.

## 1. Introduction

Determining which supercell thunderstorms are likely to produce tornadoes remains a challenging forecast problem, particularly as even the finest operational model resolutions are incapable of resolving tornadoes. To address this problem, forecasters typically rely on some combination of observed storm characteristics and known relationships between the near-storm environment and tornadoes when making short-term forecasts, watches, and warnings. While current forecasting methods based on characteristics of the near-storm environment demonstrate some forecast skill in discriminating between tornadic and nontornadic supercells, the potential exists for improvements.

Techniques that use aspects of the near-storm environment as predictors for tornado likelihood often stem from research using proximity sounding data (e.g., Fawbush and Miller 1952; Darkow 1969; Maddox 1976; Brooks et al. 1994; Rasmussen and Blanchard 1998; Thompson et al. 2003, 2007; Markowski et al. 2003; Craven and Brooks 2004; Davies 2004). Numerous sounding-derived parameters have been created based on this work to indicate the likelihood of severe weather and tornadoes [e.g., the supercell composite parameter (SCP), significant tornado parameter (STP; Thompson et al. 2002, 2003), and significant hail parameter (SHIP)]. The Sounding Analog Retrieval System (SARS; Jewell 2010) produces severe hail and tornado forecasts based on matching sounding-derived parameters from observed or forecast soundings to a proximity sounding database. Moreover, recent efforts have been made to provide conditional probabilities (provided the occurrence of a supercell) of severe weather hazards, including tornadoes, based on sounding-derived variables. For example, Togstad et al. (2011) developed two logistic regression equations based on low-level storm-relative helicity, vertical wind shear, and mixed-layer CAPE and CIN. The first regression equation, based on mixed-layer CAPE, 0–6-km wind shear, mixed-layer CIN, and 0–1-km storm relative helicity (SRH) had a chi-square score of 256.5138 and an integrated area under a relative operating characteristic (ROC; e.g., Mason 1982; Wilks 2006) curve of 0.720 for their verification dataset, while the second equation, substituting 0–1-km SRH for 0–1-km shear, had a chi-square score of 243.6602 and a ROC area of 0.718. Both equations showed modest improvement, in terms of ROC area, when compared with forecasts based on effective-layer STP (ROC area of 0.684) for their verification dataset.

*Corresponding author*: Christopher J. Nowotarski, cjnowotarski@tamu.edu

DOI: 10.1175/WAF-D-17-0189.1

A commonality among the aforementioned forecasting methods is that they all condense information from vertical wind, temperature, and moisture profiles into point parameters (e.g., SRH, CAPE, 0–1-km shear, etc.). Thus, detailed information regarding the shapes of vertical profiles may be lost in the process. Nowotarski and Jensen (2013, hereafter NJ13) demonstrated the use of self-organizing maps (SOMs) in classifying vertical profiles of *individual* sounding-derived variables of the near-storm environment toward producing conditional probability forecasts of nonsupercell storms, nontornadic supercells (NT), weakly tornadic (WT) supercells (less than F/EF2), and significantly tornadic (ST) supercells (F/EF2 or greater). While their results showed skill in discriminating among storm types, their method was limited in that each SOM could only account for one variable, and it also contained nonsupercell storms that may have clouded any potential skill in discriminating between tornadic and nontornadic supercells.

This paper extends the work of NJ13 by including profiles of *multiple* variables in each SOM and limiting the method to supercell thunderstorms with the goals of improving the forecast skill of conditional probability estimates of significant tornadoes and unearthing subtle kinematic and thermodynamic patterns in the near-storm environment associated with tornadoes. Three sets of SOMs are compared: one in which only winds are considered, one in which only thermodynamics are considered, and one in which both winds and thermodynamics are considered.

## 2. Data and methodology

The proximity sounding database used in this study is composed of the same Rapid Update Cycle-2 (RUC-2; Benjamin et al. 2004) gridpoint soundings collected, described, and used by Thompson et al. (2003, 2007) and Markowski et al. (2003) and that serve as the backbone of SARS. A total of 834 soundings are included: 443 (53.2%) associated with NT supercells, 278 (33.3%) associated with WT supercells, and 113 (13.5%) associated with ST supercells. Temperature $T$, dewpoint temperature $T_d$, and the storm-relative $u$ and $v$ wind components are interpolated to constant height levels (AGL) in 100-m increments. The reader is referred to Thompson et al. (2003) for a full discussion of the error characteristics of the RUC-2 gridpoint soundings, but it should be noted here that they discovered a tendency toward underestimated temperature and moisture near the surface and an overestimation of tropospheric winds. Consequently, there may be an underestimation of surface-based CAPE, but errors in derived shear parameters are relatively unbiased.

The SOM methodology is detailed in NJ13 and Nowotarski and Jensen (2014), but is summarized here for convenience. SOMs (Kohonen 1995) are a type of neural network that use a competitive learning algorithm to map input data vectors onto a two-dimensional map of neurons, or nodes, and can be used to objectively classify meteorological data (e.g., Jensen et al. 2012; Stauffer et al. 2016; Anderson-Frey et al. 2017). SOMs reveal patterns in the magnitude and shapes of input profiles over the depth provided in the training dataset. Because each node is connected via a neighborhood function, the SOM also maintains the topology of the dataset (i.e., adjacent nodes are more similar than distant nodes).

In this study, the vertical profiles obtained from the proximity sounding dataset serve as input or training data for each SOM. As in Nowotarski and Jensen (2014), we modify the NJ13 methodology to append additional variables to each input profile, thus doubling or (in some cases) quadrupling the length of each input data vector. A total of 60 SOMs were computed in which we compare SOMs with only thermodynamic information ($T$ and $T_d$), only kinematic information ($u$ and $v$), and a combination of thermodynamic and kinematic information ($T$, $T_d$, $u$, and $v$). Ground-relative winds are used as these were found by both Markowski et al. (2003) and NJ13 to outperform storm-relative winds in discrimination between supercell types. For each set of input variables, SOMs were computed over varying heights (1, 3, 6, and 16 km) and for different numbers and dimensions of SOM nodes ($2 \times 2$, $2 \times 3$, $3 \times 3$, $4 \times 4$, and $8 \times 2$). A second set of 60 SOMs was also computed wherein the input data were normalized using $z$ scores based on the profile average to account for differing magnitudes and units of variables, particularly in the four-variable SOMs.

## 3. Results

### a. *Evaluating SOM performance and potential forecasting skill*

Every SOM displays some degree of discrimination between environments that support NT, WT, and ST supercells. Table 1 shows the five best discriminating SOMs for NT, WT, ST, and the average for all storm types (i.e., overall) as measured by the spread between the lowest and highest nodes in the percentage of a particular storm type associated with a profile matched to that node. As described in NJ13, nodes with a large (small) percentage of a particular storm type relative to their climatological frequency are representative of a pattern in the near-storm environment with disproportionately high (low) likelihood of occurrence of that type of storm. Thus, SOMs with a large percentage spread are judged as more effective in discriminating

TABLE 1. The SOMs with the five highest percentage difference spreads (percent spread) on average and for each storm type are listed. RPSS and BSS are also listed for each SOM.

| Variables | Height (km) | Dimensions | Percent spread | BSS | RPSS |
|---|---|---|---|---|---|
| | | Overall | | | |
| $T$, $T_d$, $u$, $v$ (normalized) | 3 | 4 × 4 | 54 | 0.09 | 0.12 |
| $u$, $v$ | 1 | 4 × 4 | 50 | 0.07 | 0.10 |
| $u$, $v$ | 6 | 4 × 4 | 50 | 0.08 | 0.10 |
| $T$, $T_d$, $u$, $v$ (normalized) | 6 | 8 × 2 | 50 | 0.12 | 0.10 |
| $u$, $v$ | 3 | 8 × 2 | 49 | 0.09 | 0.11 |
| | | Nontornadic | | | |
| $u$, $v$ | 1 | 4 × 4 | 73 | 0.09 | 0.10 |
| $T$, $T_d$, $u$, $v$ (normalized) | 3 | 4 × 4 | 71 | 0.12 | 0.12 |
| $T$, $T_d$, $u$, $v$ | 6 | 4 × 4 | 70 | 0.10 | 0.10 |
| $T$, $T_d$, $u$, $v$ | 1 | 8 × 2 | 69 | 0.11 | 0.11 |
| $u$, $v$ | 1 | 8 × 2 | 68 | 0.09 | 0.10 |
| | | Weakly tornadic | | | |
| $T$, $T_d$, $u$, $v$ | 3 | 4 × 4 | 52 | 0.04 | 0.11 |
| $u$, $v$ (normalized) | 16 | 8 × 2 | 52 | 0.04 | 0.07 |
| $u$, $v$ | 3 | 8 × 2 | 48 | 0.05 | 0.11 |
| $T$, $T_d$, $u$, $v$ (normalized) | 3 | 4 × 4 | 48 | 0.04 | 0.12 |
| $u$, $v$ (normalized) | 16 | 4 × 4 | 47 | 0.05 | 0.08 |
| | | Significantly tornadic | | | |
| $u$, $v$ (normalized) | 3 | 8 × 2 | 50 | 0.12 | 0.10 |
| $T$, $T_d$, $u$, $v$ (normalized) | 6 | 8 × 2 | 46 | 0.12 | 0.10 |
| $u$, $v$ | 1 | 4 × 4 | 44 | 0.10 | 0.10 |
| $u$, $v$ | 3 | 8 × 2 | 43 | 0.13 | 0.11 |
| $T$, $T_d$, $u$, $v$ (normalized) | 3 | 4 × 4 | 43 | 0.12 | 0.12 |

between environments in which particular storm types are disproportionately common. Brier skill scores (BSSs) and the ranked probability skill score (RPSS; Wilks 2006) are included for each ranked SOM. These metrics are based on issuing storm-type probability forecasts for each profile based on the frequency of each storm type in the node to which the profile is matched. Both BSS and RPSS values vary from 0 to 1 with higher values indicating a more skillful forecast when compared with a reference forecast based on climatology (in this case, the overall storm-type frequency). Somewhat surprisingly, for all SOMs, normalized SOMs had the same average percentage spread (31%) as those not normalized, and skill scores were generally indistinguishable.[1] Considering these similarities, results from both sets of SOMs are shown below.

For all storm types, the best-performing SOMs are those that include kinematic information (regardless of if they also include thermodynamic data), which is consistent with results from NJ13. Contrastingly, no SOMs containing *only* thermodynamic information are ranked highly, suggesting they are a less effective discriminator. For all 120 SOMs the average overall percentage spread for $u$ and $v$ SOMs (37%) and $T$, $T_d$, $u$, and $v$ SOMs (35%) is higher than for $T$ and $T_d$ SOMs (22%). Both BSS and RPSS metrics are considerably lower for $T$ and $T_d$ SOMs as well. Indeed, the average BSS and RPSS are both highly correlated ($r \approx 0.9$) with average percentage spread. Additionally, relatively shallow SOMs perform best overall with average percentage spread maximized for 3-km SOMs. SOMs with a greater number of nodes perform best overall, regardless of variables considered or height, with 4 × 4 and 8 × 2 SOMs having higher percentage spreads (40% and 41%, respectively) on average than the next highest category (3 × 3 SOMS; 30%).[2] Kohonen (1995) suggests that despite the same number of nodes, rectangular SOMs learn more effectively. Indeed, in this study the 8 × 2 SOMs slightly outperform the 4 × 4 SOMs in all metrics, though the differences are minor when compared with those seen when varying the total number of nodes.

[1] It is likely that the normalized SOMs would outperform the nonnormalized SOMs for variables where the mean and standard deviation of the profiles are considerably different from each other; however, for the variables used in this study the magnitude and variability of the profiles are similar, even despite different units.

[2] Though this trend might provide an argument for SOMs with an even greater number of nodes, SOMs with more than 16 nodes often result in outlier nodes wherein an insignificant number of events match each node.

Qualitatively, the overall results discussed above tend to apply to individual storm-type categories as well. Interestingly, the average BSS tends to be maximized for NT (BSS = 0.06) and ST (BSS = 0.06) storm types, suggesting WT (BSS = 0.03) storm environments share commonalities with both NT and ST environments and may be hard to differentiate. Moreover, the best WT SOMs tend to consider a greater depth of the atmosphere than those resulting in higher BSSs for NT and WT storm types.

Since the bulk of existing forecasting parameters and efforts are geared toward forecasting significant tornadoes, the remainder of this analysis will focus on multivariate SOM skill in discerning the ST storm-type likelihood. ST skill improves markedly when only including the lowest half of the troposphere. The best ST BSS is 0.13 while the highest ST percentage spread is 50%. For ST storm types, the ST BSS and ST percentage spread in all SOMs are strongly positively correlated ($r$ = 0.89), reinforcing the notion that both BSS and percentage spread are reasonable metrics for SOM performance.

Another metric of potential forecasting skill is the ROC curve area, where an area of zero equates to no forecast skill (false alarm and hit rates are equivalent) whereas an area of one indicates a perfect forecast. The highest ROC area for ST probability forecasts is 0.77 (Fig. 1a), and the ROC area tends to be lower for SOMs that only include thermodynamic data. Moreover, across all SOMs the ST percentage spread and ROC area for ST forecasts are highly correlated ($r$ = 0.87). Togstad et al. (2011) showed that, for their dataset, their regression equations resulted in ST conditional probability forecasts with ROC areas of 0.720 and 0.718, which outperformed the effective-layer STP (0.684). For our dataset, the Togstad et al. equations resulted in ROC areas of 0.71 and 0.73. The best-performing SOM, in terms of ROC area, in this study was the 3 km AGL, 8 × 2, $u$ and $v$ nonnormalized SOM with a ROC area of 0.77, suggesting that the SOM technique may potentially yield modestly higher skill than existing methods, particularly at lower probability decision thresholds (Fig. 1b).

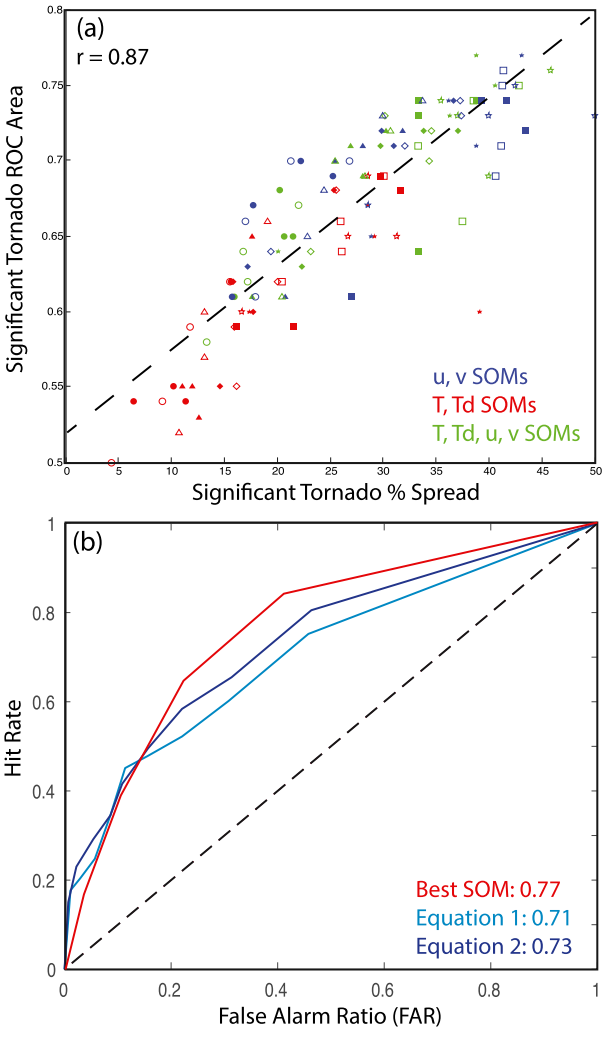


FIG. 1. (a) Scatterplot of ST percentage spread and ROC area for ST probability forecasts for each SOM color coded by the variables included in each SOM. Filled markers represent nonnormalized SOMs while open markers represent normalized SOMs. Circles represent 2 × 2 SOMs, triangles represent 2 × 3 SOMs, diamonds represent 3 × 3 SOMs, squares represent 4 × 4 SOMs, and stars represent 8 × 2 SOMs. The black dashed line indicates the linear best fit. (b) ROC curve for ST probability forecasts derived from the 3-km, 8 × 2, $u$ and $v$ nonnormalized SOM (red) and logistic regression equations from Togstad et al. (2011) (blue).

### b. *SOM attributes*

Perhaps the greatest value of SOMs is their ability to discern distinct patterns in hodographs and thermodynamic profiles, particularly at low levels, which may be washed out by simpler methods such as averaging profiles by storm type. Thus, in this section we examine output from two of the best-performing SOMs for ST near-storm environment discrimination.

#### 1) 0–1-KM WIND SOM

The 0–1 km AGL, 4 × 4, $u$ and $v$ nonnormalized SOM is one of the SOMs with the highest ST percentage spreads and ranks highly overall and in the NT and ST categories (Table 1). By including vertical profiles of the horizontal wind components, this SOM effectively classifies based on hodograph shape, as shown in Fig. 2. Moving from left to right across the SOM, hodograph length increases, while moving from top to bottom shear transitions from westerly to southerly (or even southeasterly). In general, nodes on the top-left side of the SOM are more favorable for NT types, whereas nodes on the right side of the SOM are more favorable for ST storm types. In the center of SOM, nodes tend to be

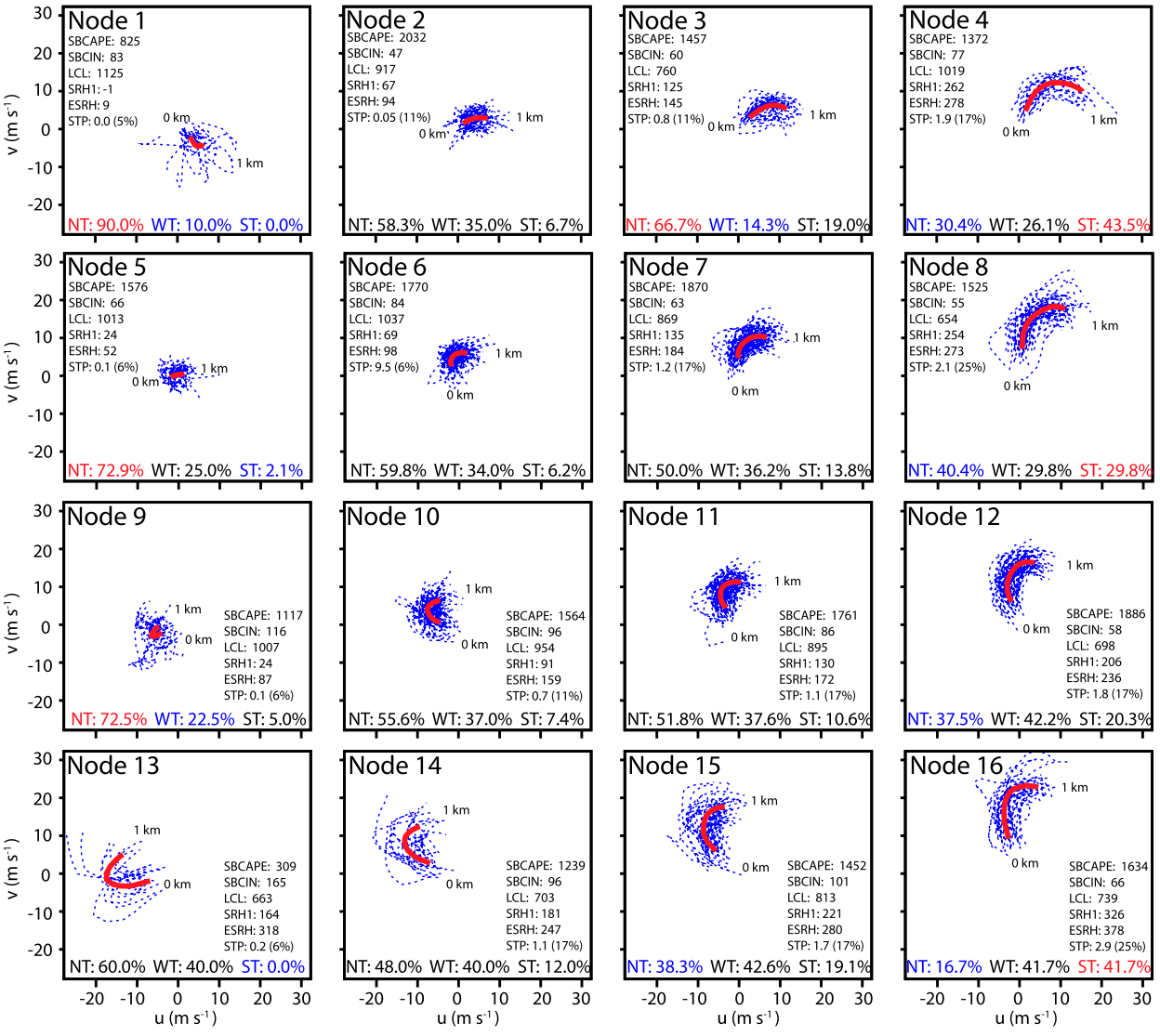


FIG. 2. Nodes from the 0–1-km, 4 × 4, $u$ and $v$ SOM showing each hodograph matching the node (dashed blue) and the average of all cases matching the node (red). Percentages of each storm type composing the node are included, highlighted by red when the percentage exceeds the climatological frequency by more than 10% and in blue when less than the climatological frequency by more than 10%. Composite convective parameters are shown for each node, including surface-based CAPE (SBCAPE; J kg$^{-1}$), surface-based CIN (SBCIN; J kg$^{-1}$), LCL (m), 0–1-km SRH (SRH1; m$^2$ s$^{-2}$), effective-layer SRH (ESRH; m$^2$ s$^{-2}$), and fixed-layer STP with the conditional probability (given a supercell) of a significant tornado occurring based on STP (Smith et al. 2015).

fairly indiscriminate of storm type (i.e., the frequencies of each storm type are similar to their climatological averages). The strongest ST nodes (nodes 4 and 16) display distinctly different low-level hodograph shapes, which would not be evident had all the ST hodographs simply been averaged.

Figure 3 clearly highlights the power of the SOM to produce nodes that discriminate between storm types. Nodes with large, positive (negative) percentage differences (red bars) indicate the frequency of that storm type is much higher (lower) than in the climatology as a whole. From a forecasting perspective, a remaining challenge of the SOM technique is highlighted by the fact that the least discriminative nodes (e.g., nodes 6, 7, 10, and 11) tend to have the highest numbers of matching profiles (blue bars), suggesting that many profiles may not be matched to nodes with a clear tendency toward a particular storm type. Conditional probability forecasts based on fixed-layer STP (Smith et al. 2015) tend to under- (over) predict ST likelihood for nodes with a high (low) frequency of ST storms.

For many nodes in this SOM, both geographic and temporal patterns also emerge (Fig. 4). For instance, one

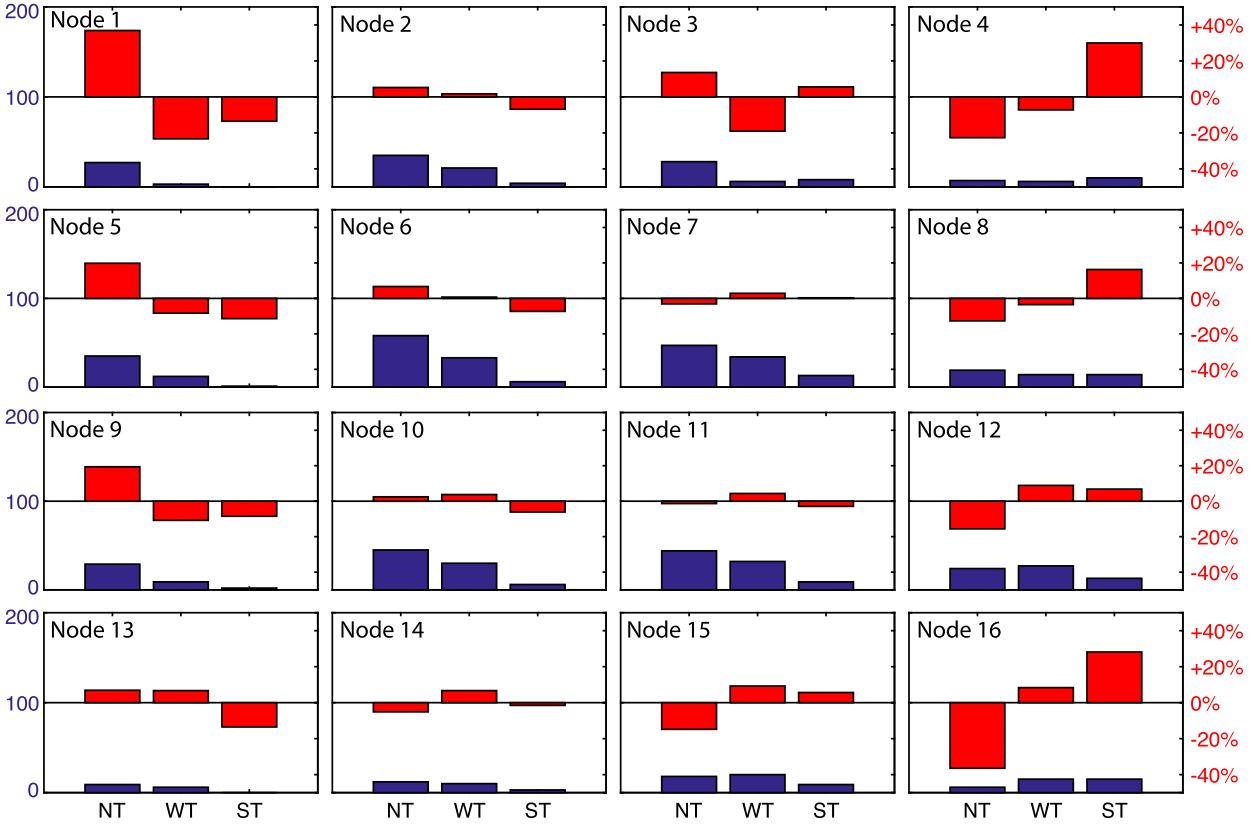


FIG. 3. Bar graphs for each node in Fig. 2 showing the total number of each storm type in a node (blue) and percentage difference relative to the overall climatology (red).

ST node (node 4) tends to occur between 2000 and 0200 UTC from the late spring through fall time period in the Mississippi and Ohio River valleys and the Midwest. This node is typified by long-curving hodographs with westerly 0–1-km shear. Another ST dominant node (node 16) tends to occur over a larger range of times of day than node 4, yet is confined to the winter and spring months. This node has events focused over the central and southern plains and lower Mississippi valley. Meteorologically, this cluster is associated with strong southerly low-level shear, perhaps indicative of the strong low-level jet often linked to tornadoes in this region. Nodes 8 and 12 are interesting in that they both have a reduced number of NT supercells relative to the overall climatology, yet node 8 is more significantly tornadic than node 12 (Figs. 2 and 3). Though both nodes have similar spatial and temporal distributions (Fig. 4), and similar hodograph shapes (Fig. 2), node 8 has a slightly longer 0–1-km hodograph owing to additional low-level veering of the winds and correspondingly larger SRH and STP. Nodes 1 and 9 are both dominated by NT supercells, and (unsurprisingly) both have hodographs with weak low-level shear. However, low-level winds in node 1 tend toward the bottom-right quadrant of the hodograph (northwest winds) while those in node 9 tend toward the bottom-left quadrant (northeast winds). This discrepancy may explain the notable geographic distribution of both nodes, wherein node 1 is focused on the northern tier of the continental United States (CONUS) and node 9 tends toward the high plains. A number of patterns associated with other storm types and hodograph shapes exist in other nodes, as well.

### 2) 0–6-KM WIND, TEMPERATURE, AND DEWPOINT SOM

Though not quite as skillful at detecting ST patterns as the aforementioned SOM, the 0–6 km AGL, $4 \times 4$, $T$, $T_d$, $u$, and $v$ nonnormalized SOM is one of the best-performing four-variable SOMs. Figure 5 shows the characteristics of nodes with the highest NT percentage (node 1), a node that discriminates well for WT storm types (node 4), and two ST-dominant nodes (nodes 12 and 16). This SOM reveals different patterns in both the deep-layer hodograph and thermodynamic profiles, wherein the NT node has northwesterly shear with

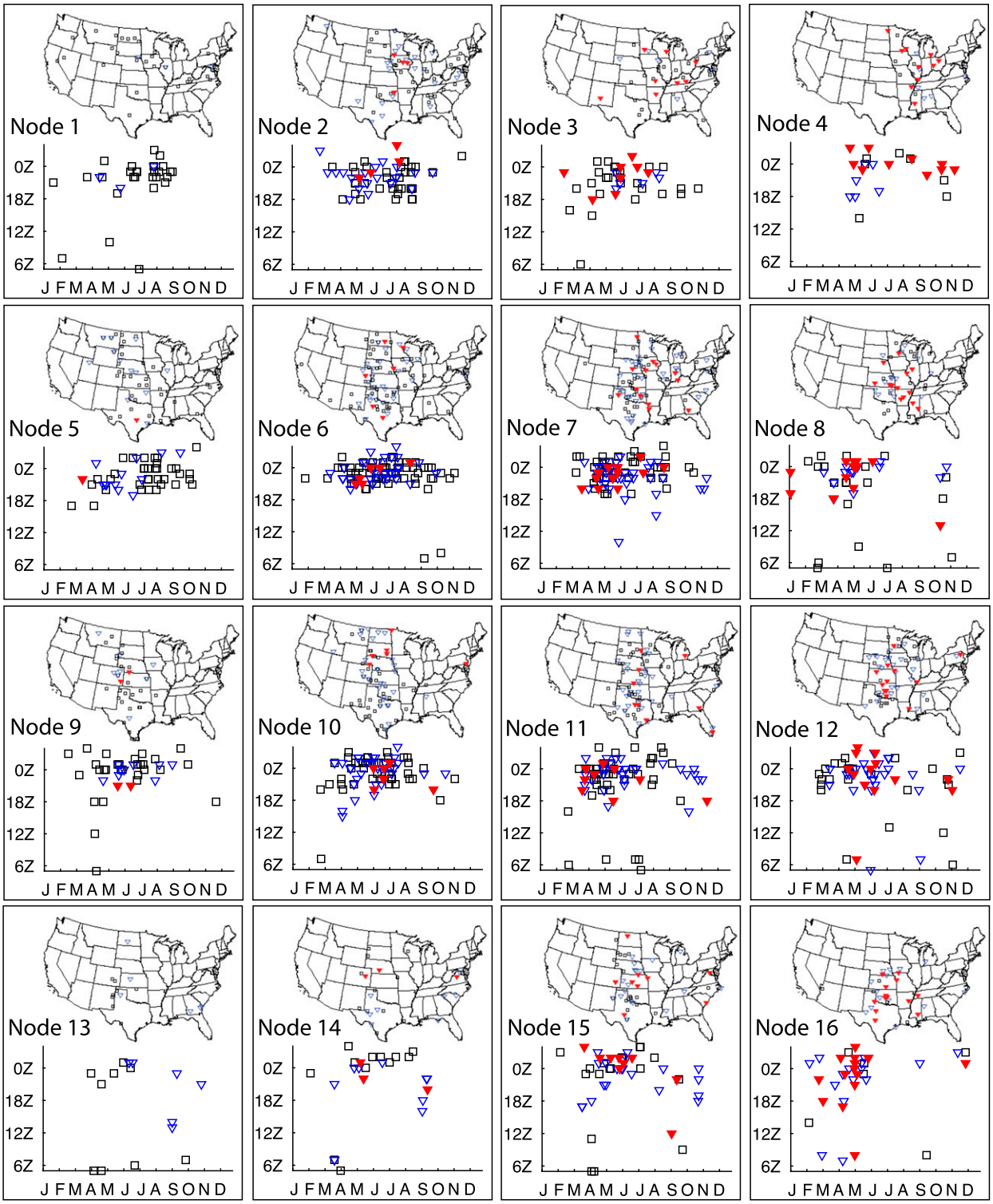


FIG. 4. Maps and scatterplots of month and time of day for each node in Fig. 2 showing the distributions of NT (open black squares), WT (open blue wedges), and ST (solid red wedges) supercells.

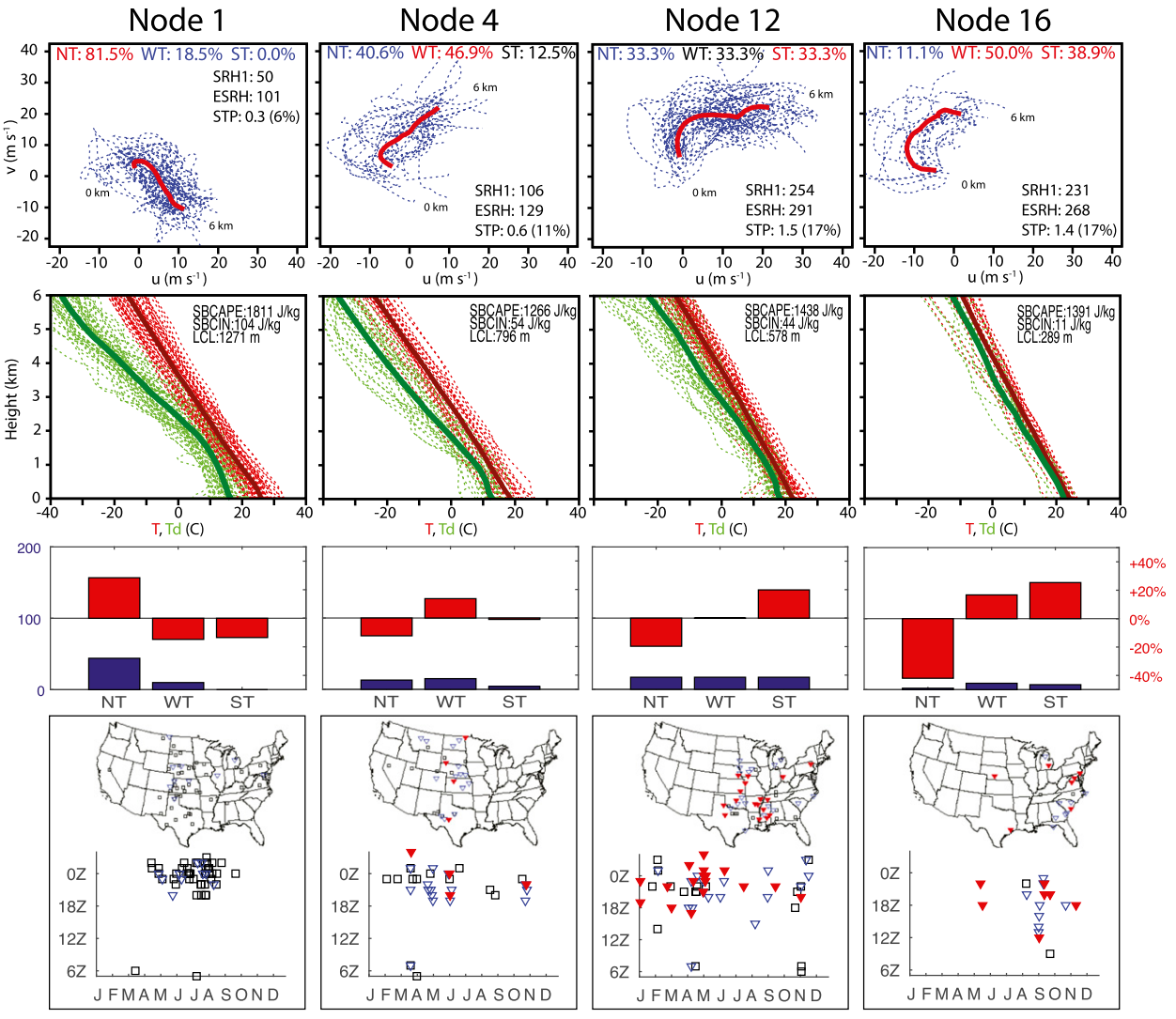


FIG. 5. As in Figs. 1–4, but showing characteristics of four nodes selected from the 0–6-km, 4 × 4, $T$, $T_d$, $u$, and $v$ SOM.

limited low-level curvature. The WT node has a similar shape and length as the NT node; however it is characterized by southwesterly shear, cooler temperatures, and greater moisture, resulting in a lower lifting condensation level (LCL). The cooler temperatures in node 4 may arise from a generally higher-elevation region in this node in the high plains and Intermountain West, while node 1 has a wider geographic range and matches generally occurring during the summer months.

The hodographs for the two ST nodes are easily distinguished from each other. Node 12 is similar to the average ST hodograph from Markowski et al. (2003) due to the southerly low-level shear turning to westerly aloft. On the other hand, node 16 (with notably fewer members) is characterized by easterly low-level shear, with considerably more curvature over the full 6-km depth. Despite similar temperatures and stability, node 16 displays a considerably more moist thermodynamic profile with a very low average LCL (289 m). Interestingly, though rare, the node 16 cases tend to have a wide geographic distribution and occur primarily during the fall months, whereas the node 12 cases tend to follow geographic and temporal distributions typical of the overall U.S. tornado climatology.

## 4. Conclusions

This study expands on the earlier work of NJ13 to include multiple variables in the SOM classification algorithm. The results suggest that the greatest discrimination between storm types, and therefore the greatest potential forecasting skill, exists for SOMs that include

wind information, whereas SOMs that are limited to only thermodynamic information perform relatively poorly. Potential utility for forecasting weakly tornadic supercells is diminished relative to nontornadic and significantly tornadic storms, suggesting these events may be intrinsically more difficult to predict. Distinct hodograph shapes emerge among SOM nodes even for nodes with the same dominant storm types, suggesting that classification based only on resultant storm type may obscure multiple environmental modes that may produce significant tornadoes. Finally, though modest, some improvement in forecast skill over existing methods may be obtainable through the use of multivariate SOMs in operational forecasting.

The next step in integrating SOM classification of near-storm environments into operational tornado forecasting is the creation of a real-time conditional probability nowcast/forecast product. Such a product would ingest gridpoint soundings from high-resolution model analyses and/or forecasts (e.g., the Real-Time Mesoscale Analysis or High Resolution Rapid Refresh model) and match each gridpoint sounding to a node from one of (or several of) the best-performing SOMs identified in this study. Based on the frequency of each storm type from the training dataset occurring in the node(s), a conditional probability of a tornadic (WT + ST) or ST supercell would thus be obtained for each grid point. These probabilities could then be contoured on a map display, similar to existing products on the Storm Prediction Center mesoanalysis. Ideally, such a system would improve with time as new cases are added to the training dataset.

*Acknowledgments.* We wish to thank Roger Edwards and Rich Thompson for providing the proximity sounding dataset used in this work. We also thank Dr. Anders Jensen for input and providing initial versions of the code used to generate SOMs. Dr. Rob Warren provided some useful insight on normalizing SOM data and sensitivity to SOM dimensions. We also thank the Laboratory of Computer and Information Science Adaptive Informatics Research Centre at the Helsinki University of Technology for providing and maintaining the MATLAB SOM Toolbox. SHARPpy sounding software (Blumberg et al. 2017) was used for the calculation of composite convective parameters. Finally, we thank three anonymous reviewers for their helpful comments. This work is funded, in part, by NSF Grant AGS-1446342 through the NSF Physical and Dynamic Meteorology program. Support for E. Jones was provided through the Atmospheric Science in the Gulf Coast Region Research Experience for Undergraduates program at Texas A&M University in College Station, Texas, sponsored by NSF Grant AGS-1559895.

## REFERENCES

Anderson-Frey, A. K., Y. P. Richardson, A. R. Dean, R. L. Thompson, and B. T. Smith, 2017: Self-organizing maps for the investigation of tornadic near-storm environments. *Wea. Forecasting*, **32**, 1467–1475, https://doi.org/10.1175/WAF-D-17-0034.1.

Benjamin, S. G., and Coauthors, 2004: An hourly assimilation–forecast cycle: The RUC. *Mon. Wea. Rev.*, **132**, 495–518, https://doi.org/10.1175/1520-0493(2004)132<0495:AHACTR>2.0.CO;2.

Blumberg, W. G., K. T. Halbert, T. A. Supinie, P. T. Marsh, R. L. Thompson, and J. A. Hart, 2017: SHARPpy: An open-source sounding analysis toolkit for the atmospheric sciences. *Bull. Amer. Meteor. Soc.*, **98**, 1625–1636, https://doi.org/10.1175/BAMS-D-15-00309.1.

Brooks, H. E., C. A. Doswell III, and J. Cooper, 1994: On the environments of tornadic and nontornadic mesocyclones. *Wea. Forecasting*, **9**, 606–618, https://doi.org/10.1175/1520-0434(1994)009<0606:OTEOTA>2.0.CO;2.

Craven, J. P., and H. E. Brooks, 2004: Baseline climatology of sounding derived parameters associated with deep, moist convection. *Natl. Wea. Dig.*, **28**, 13–24.

Darkow, G. L., 1969: An analysis of over sixty tornado proximity soundings. Preprints, *10th Conf. on Severe Local Storms*, Omaha, NE, Amer. Meteor. Soc., 218–221.

Davies, J. M., 2004: Estimations of CIN and LFC associated with tornadic and nontornadic supercells. *Wea. Forecasting*, **19**, 714–726, https://doi.org/10.1175/1520-0434(2004)019<0714:EOCALA>2.0.CO;2.

Fawbush, E. J., and R. C. Miller, 1952: A mean sounding representative of the tornadic air-mass environment. *Bull. Amer. Meteor. Soc.*, **33**, 303–307.

Jensen, A. A., A. M. Thompson, and F. J. Schmidlin, 2012: Classification of Ascension Island and Natal ozonesondes using self-organizing maps. *J. Geophys. Res.*, **117**, D04302, https://doi.org/10.1029/2011JD016573.

Jewell, R. E. D., 2010: A sounding analog system to produce probabilistic forecasts of maximum hail size. Preprints, *25th Conf. on Severe Local Storms*, Denver, CO, Amer. Meteor. Soc., 4B.3, https://ams.confex.com/ams/25SLS/techprogram/paper_176260.htm.

Kohonen, T., 1995: *Self-Organizing Maps.* Springer, 362 pp.

Maddox, R. A., 1976: An evaluation of tornado proximity wind and stability data. *Mon. Wea. Rev.*, **104**, 133–142, https://doi.org/10.1175/1520-0493(1976)104<0133:AEOTPW>2.0.CO;2.

Markowski, P. M., C. Hannon, J. Frame, E. Lancaster, A. Pietrycha, R. Edwards, and R. L. Thompson, 2003: Characteristics of vertical wind profiles near supercells obtained from the Rapid Update Cycle. *Wea. Forecasting*, **18**, 1262–1272, https://doi.org/10.1175/1520-0434(2003)018<1262:COVWPN>2.0.CO;2.

Mason, I., 1982: A model assessment of weather forecasts. *Aust. Meteor. Mag.*, **30**, 291–303.

Nowotarski, C. J., and A. A. Jensen, 2013: Classifying proximity soundings with self-organizing maps toward improving supercell and tornado forecasting. *Wea. Forecasting*, **28**, 783–801, https://doi.org/10.1175/WAF-D-12-00125.1.

——, and ——, 2014: Objective classification of supercell environments using multivariate self-organizing maps for research and forecasting. *27th Conf. on Severe Local Storms*, Madison, WI, Amer. Meteor. Soc., 12.B3, https://ams.confex.com/ams/27SLS/webprogram/Paper254697.html.

Rasmussen, E. N., and D. O. Blanchard, 1998: A baseline climatology of sounding-derived supercell and tornado forecast parameters. *Wea. Forecasting*, **13**, 1148–1164, https://doi.org/10.1175/1520-0434(1998)013<1148:ABCOSD>2.0.CO;2.

Smith, B. T., R. L. Thompson, A. R. Dean, and P. T. Marsh, 2015: Diagnosing the conditional probability of tornado damage rating using environmental and radar attributes. *Wea. Forecasting*, **30**, 914–932, https://doi.org/10.1175/WAF-D-14-00122.1.

Stauffer, R. M., A. M. Thompson, and G. S. Young, 2016: Tropospheric ozonesonde profiles at long-term U.S. monitoring sites: 1. A climatology based on self-organizing maps. *J. Geophys. Res. Atmos.*, **121**, 1320–1329, https://doi.org/10.1002/2015JD023641.

Thompson, R. L., R. Edwards, and J. A. Hart, 2002: Evaluation and interpretation of the supercell composite and significant tornado parameters at the Storm Prediction Center. Preprints, *21st Conf. on Severe Local Storms/19th Conf. on Weather Analysis and Forecasting/15th Conf. on Numerical Weather Prediction*, San Antonio, TX, Amer. Meteor. Soc., J3.2, https://ams.confex.com/ams/pdfpapers/46942.pdf.

——, ——, ——, K. L. Elmore, and P. Markowski, 2003: Close proximity soundings within supercell environments obtained from the Rapid Update Cycle. *Wea. Forecasting*, **18**, 1243–1261, https://doi.org/10.1175/1520-0434(2003)018<1243:CPSWSE>2.0.CO;2.

——, C. M. Mead, and R. Edwards, 2007: Effective storm-relative helicity and bulk shear in supercell thunderstorm environments. *Wea. Forecasting*, **22**, 102–115, https://doi.org/10.1175/WAF969.1.

Togstad, W. E., J. M. Davies, S. J. Corfidi, D. R. Bright, and A. R. Dean, 2011: Conditional probability estimation for significant tornadoes based on Rapid Update Cycle (RUC) profiles. *Wea. Forecasting*, **26**, 729–743, https://doi.org/10.1175/2011WAF2222440.1.

Wilks, D. S., 2006: *Statistical Methods in the Atmospheric Sciences.* 2nd ed. Academic Press, 627 pp.